Magnetometers and electro-magnetometers

I. J. Won and Haoping Huang, Geophex, Ltd., Raleigh, North Carolina, U.S.

A magnetometer is used in a geophysical survey to measure magnetic susceptibility variations in earth. It is a passive sensor because it uses the ambient earth magnetic field as the source of excitation.

An electromagnetic (EM) sensor operating below the radio frequency (RF), or in an EM induction (EMI) mode, is commonly used to measure electrical conductivity variations in earth. (An EM sensor operating above the RF, commonly called ground-probing radar or GPR, can measure variations in dielectric permittivity, which we do not consider here.) For this reason, an EMI sensor is often called a *conductivity meter*. It is an active sensor because it carries its own source of excitation.

It has been common to consider that a magnetometer is the principal sensor for measuring magnetic susceptibility, and that an EMI sensor is the principal sensor for measuring electrical conductivity. Discussions of EMI in many geophysics textbooks often start with "Let us assume that the magnetic permeability is that of free space…" or similar sentences that dismiss the role of susceptibility in EMI physics. Such discussions, as well as historical limitations in the sensor technologies, have promoted the notion that magnetometers and EMI sensors have separate and distinct functions for measuring each physical property.

It is well known, however, that an EMI sensor responds to both electrical conductivity *and* magnetic susceptibility. In fact, an EMI sensor operating at sufficiently low frequencies acts more as a magnetometer than as a conductivity meter. At the so-called "resistive limit" where the conductivity-frequency product is small, an EMI sensor responds only to magnetic susceptibility and ignores electrical conductivity. It would be a serious misnomer in this case to call an EMI sensor a conductivity meter. A correct designation would be an *active magnetometer* or, as we propose here, an *electro-magnetometer*. A properly designed electro-magnetometer can serve two simultaneous functions: that of a magnetometer *and* of a conductivity meter.

Magnetometers and susceptibility. As a simple discussion, consider a vertical magnetic field having a magnitude Hz impinging on a uniform half-space having a magnetic susceptibility κ. The permeable half-space generates a vertical magnetic anomaly ΔH_z such that

$$\Delta H_z = 2\pi\kappa \, H_z. \qquad (1)$$

For a given H_z, therefore, ΔH_z is strictly proportional to κ and independent of the sensor height above the earth. This is a simple theoretical basis for claiming that a magnetic anomaly map is equivalent to an *apparent* magnetic susceptibility map, where the word *apparent* is needed for the assumption of half-space uniformity.

Strictly speaking, this relation applies only to the vertical field measurable by a vector magnetometer (a fluxgate magnetometer, for instance), which is rarely used in modern geophysical surveys due to its excessive orientation sensitivity. Total-field magnetic data are much more common today
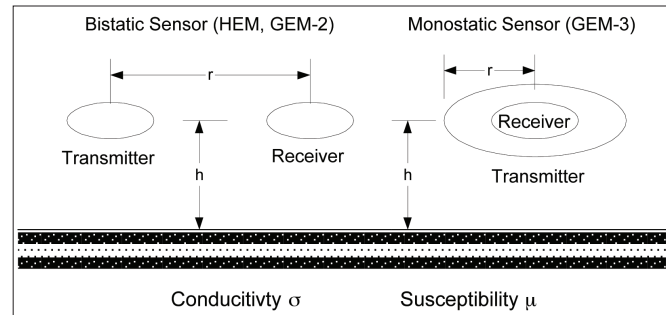

Figure 1. *Two types of EM sensors above a half-space: bistatic (left) and monostatic (right).*

because of many commercial optical-pump types of scalar magnetometers with high resolutions.

A total-field magnetic anomaly exhibits a dipolar anomaly pattern (i.e., a combination of high and low amplitudes) for an isolated object located anywhere other than at the magnetic poles. Locating the anomaly source on this dipolar pattern is not easy because the source is somewhere between the high and the low. The task would be easy, however, had the anomaly been obtained at the poles; then the anomaly would be monopolar, and the source would be simply located at the center of the anomaly. A numerical process known as "reduction to pole" is sometimes used to move the survey data *mathematically* to the North Pole where a dipolar anomaly turns into a monopolar anomaly, which helps interpretation.

As will be explained in the next section, a vertical EM dipole as an illuminating source provides an *artificial* North Pole condition, which produces reduced-to-pole data that would be directly applicable to equation 1 without further processing.

Electromagnetometers and susceptibility. EMI sensors are some of the oldest geophysical sensors. They are generally classified into frequency-domain (FD) and time-domain (TD) sensors. We will mainly consider here the FD sensors that can operate in a broad bandwidth, particularly at low frequencies that qualify as the resistive limit. Such EMI sensors can act both as a magnetometer and as a conductivity meter. TD sensors with multiple time windows, including very late-time channels, would also be qualified for a similar double function.

Consider an EMI sensor consisting of a set of transmitter and receiver coils placed above a uniform half-space having a conductivity σ and susceptibility κ. There can be several variations in configuring the transmitter and receiver coils. Figure 1 shows two common configuration examples: *bistatic* or separated coplanar coils such as all helicopter-towed EMI (HEM) sensors used for mineral exploration and several commercial handheld EMI sensors and *monostatic* or collocated coplanar coils.

The ratio T between the secondary field H_S against the primary field H_P at the receiver coil can be expressed as (for example, see Ward and Hohmann, 1988):

$$T \equiv \frac{H_s}{H_p} = c \int_0^\infty \frac{u - \lambda}{u + \lambda} \lambda^n e^{-2\lambda h} J_k(\lambda r) d\lambda \, ; \, u = \frac{\mu_0}{\mu}\sqrt{\lambda^2 + i\omega\mu\sigma} \qquad (2)$$
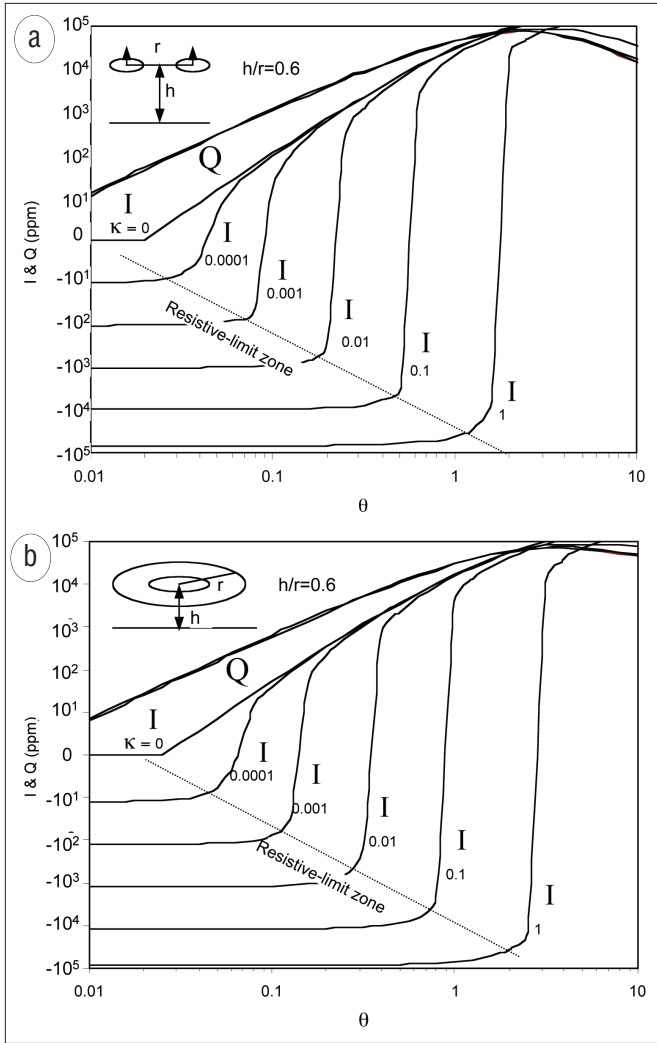
Figure 2. Computed in-phase (I) and quadrature (Q) responses of a homogeneous half-space plotted as a function of induction number θ for various values of the magnetic susceptibility κ, for (a) horizontal coplanar and (b) concentric coil configurations. The Q components are indistinguishable for the entire range of κ.

Figure 3. Percent precision of the susceptibility calculation as functions of the susceptibility κ and the product of frequency and conductivity σf for (a) horizontal coplanar and (b) concentric coil configurations.

where h is the sensor height, ω the angular frequency, and J_k the Bessel function of k-th order. The half-space magnetic permeability μ is related to the susceptibility κ and the free-space permeability μ_0 through $\mu = \mu_0 (1 + \kappa)$. The values for c, k, and n in equation 2 depend on the coil configurations: for *bistatic horizontal coplanar*, $c=r^3$, $n=2$, and $k=0$; for *bistatic vertical coplanar* or *monostatic coplanar*, $c=r^2$, $n=1$, and $k=1$.

The complex ratio T, when multiplied by 10^6, is in a unit of parts-per-million (ppm) and consists of the real (in-phase, I) and imaginary (quadrature, Q) components. Figure 2 shows the computed I and Q as a function of induction number θ, defined by $\theta = (\omega\sigma\mu/2)^{1/2}r$ for various values of κ for a bistatic horizontal coplanar configuration (2a) and for a monostatic coplanar configuration (2b). Figure 2b is also applicable to a bistatic vertical coplanar configuration. As noted in both graphs, the I component is highly dependent on κ, while Q remains basically the same over a broad range of θ.

The resistive-limit zones (the lower left corners) are where the magnetization effect dominates the EM response, which is in phase with the primary field but in an opposite polarity, according to Lenz's law. Within the resistive-limit zone, the in-phase is independent of the induction number and, in turn, of frequency. This property can be used to convert the quadrature data to apparent conductivity at two frequencies in mag-
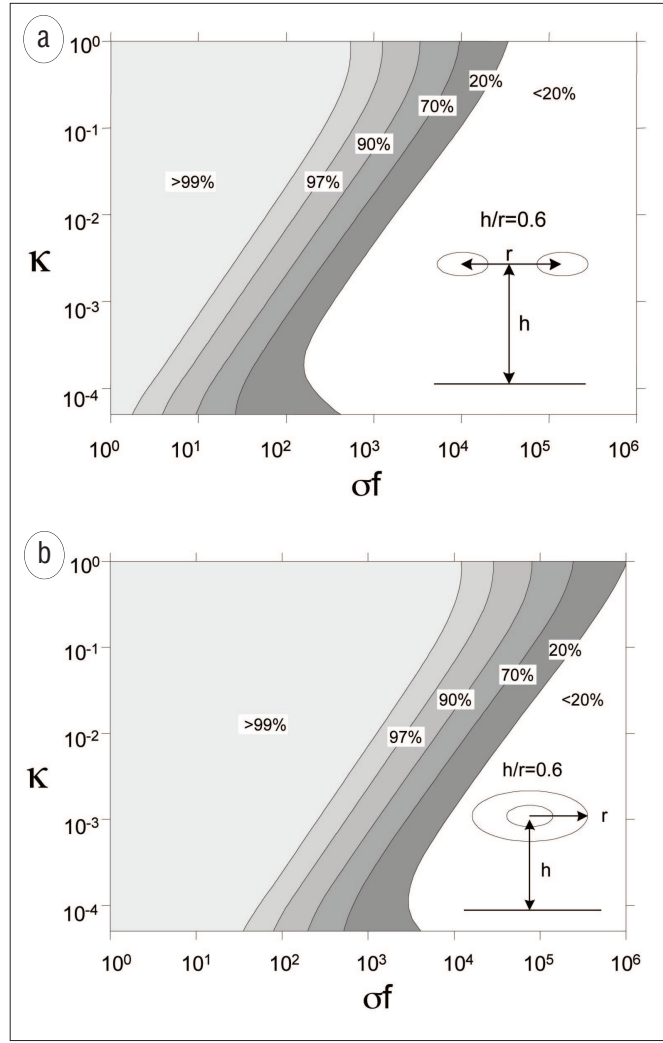
netic environments (Huang and Fraser, 1998, 2000, and 2001; Huang and Won, 2000). The resistive-limit zone varies with the susceptibility: for bistatic coplanar coils, for instance, the zone is below $\theta <0.025$ for $\kappa=0.0001$ while $\theta<2$ for $\kappa=1$. For most handheld sensors, all natural geologic features can be considered the resistive-limit at the sensors' lowest operating frequencies.

The precision of the resistive-limit assumption can be assessed from equation 2 by computing the integral T for various pairs of (σf, κ) and comparing it with the T when $\sigma f=0$. Figure 3 shows the precision of the susceptibility calculation as functions of σf and κ for the two coil configurations. For instance, if a monostatic sensor operates at 90 Hz over a ground having a conductivity of 0.1 S/m ($\sigma f=9$), we note the precision exceeds 99% for the entire range of κ. For a bistatic sensor, on the other hand, the precision is better than 90% for $\kappa<0.001$, while better than 99% for $\kappa>0.001$.

While the integral T is, in general, complex, it becomes real at the resistive limit as the product wσ approaches zero, where $u \approx (\mu_0/\mu)\lambda = \lambda/(1 + \kappa)$. T then becomes

$$T = \frac{-\kappa}{2 + \kappa} c \int_0^\infty \lambda^n e^{-2\lambda h} J_k(\lambda r) d\lambda = \frac{-\kappa}{2 + \kappa} G \cong -\frac{\kappa}{2} G \quad (3)$$

where G denotes an integral that only depends on the coil configuration. The last approximation comes from the fact that magnetic susceptibility is small. In fact, it rarely exceeds 0.01
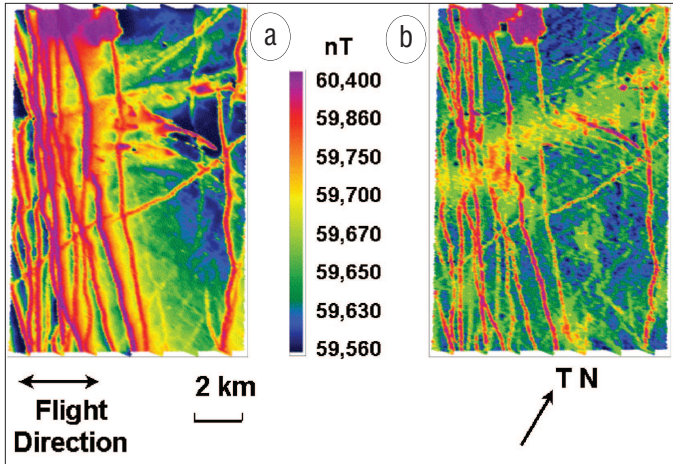
Figure 4. EM and magnetic data obtained by a Dighem HEM system in northern Canada: (a) total field magnetometer data; (b) apparent susceptibility derived from 900Hz EM data. From Huang and Fraser (2000).
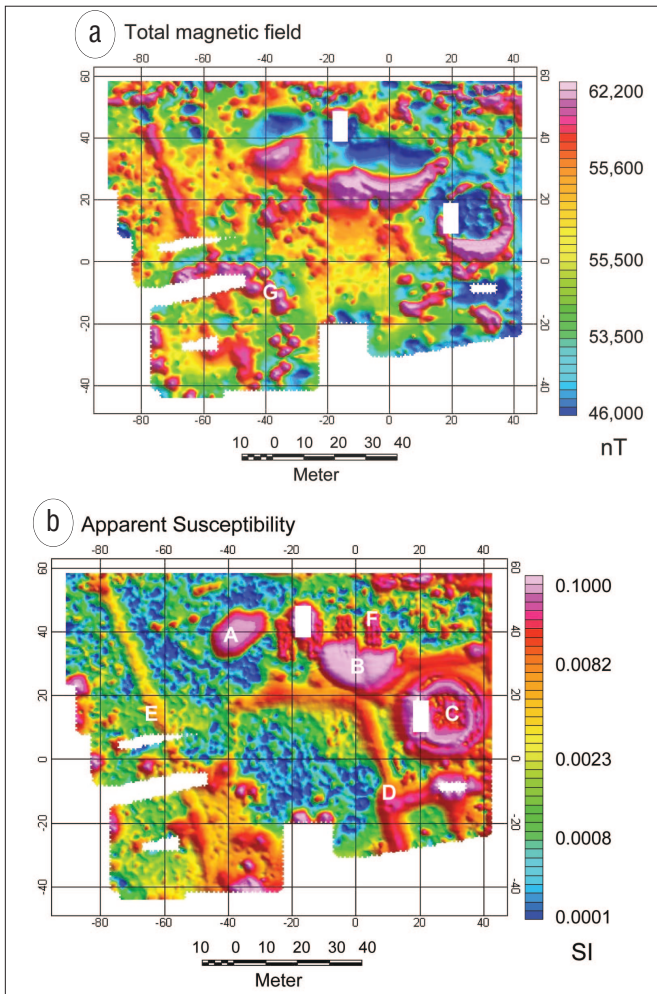

Figure 5. Field data from a defunct manufactured gas plant in New England: (a) the total field magnetometer data; (b) apparent susceptibility derived from 1050 Hz GEM-2 data.

in nature. Two significant points are: T is real, i.e., in-phase and T is linearly proportional to κ. Finally, the integral G can be shown for the *bistatic horizontal coplanar* coils configuration:

$$G = \frac{8(h/r)^2 - 1}{[4(h/r)^2 + 1]^{5/2}} \cong \frac{1}{4}\left(\frac{r}{h}\right)^3 \quad for \ r << h \quad (4)$$

and for either *bistatic vertical* configuration or *monostatic coplanar* configuration:

$$G = \frac{1}{[4(h/r)^2 + 1]^{3/2}} \cong \frac{1}{8}\left(\frac{r}{h}\right)^3 \quad for \ r << h . \quad (5)$$

The approximations are when the sensor height is much greater than the coil geometry, such as for an airborne sensor. Equation 3 indicates that the in-phase is linearly proportional to half-space magnetic susceptibility, which is the basis for an EMI sensor, when operated in a *resistive limit* (i.e., at a sufficiently low frequency), to become a magnetometer. We designate the EMI sensor at this stage as an *electro-magnetometer*.

The major disadvantage of an electro-magnetometer employing a dipole magnetic source is that it attenuates by approximately a factor of distance-cubed faster than a magnetometer, indicated by equations 1, 3, 6, and 7. This factor is attributed to the attenuation of a magnetic dipole used as the illumination source. Therefore, an electro-magnetometer is mainly useful for shallow investigations. On the other hand, this attenuation can be turned into an advantage in producing a higher spatial resolution for near-surface targets that are common in environmental and engineering investigations, including unexploded ordnance and land mines.

As another advantage, an electro-magnetometer produces a reduced-to-pole magnetic anomaly as explained in the previous section. The transmitter, commonly a vertical magnetic dipole to render maximum ground coupling, provides a vertical magnetic field directly below the sensor. Unlike a magnetometer, an electro-magnetometer always produces a monopolar anomaly anywhere, regardless of magnetic latitude, which renders the task of locating the anomalous source simple.

Field data examples. We present a data example for each sensor type, where we compare the magnetometer data with the apparent susceptibility data derived from an electro-magnetometer. Strictly speaking, the magnetic data should be reduced to pole (using 2D gridded data) before comparison, which is not done in these examples mainly for the reason of simplicity.

1) Helicopter-borne Dighem HEM data. The first example comes from a published article by Huang and Fraser (2000). A Dighem HEM sensor flew over a northern Canada site to produce both a magnetic map from a cesium-vapor magnetometer and an apparent susceptibility map derived from 900 Hz in-phase data (Figure 4). The authors state that the similarity between the two maps is expected because the geology is steeply dipping with thin overburden. Therefore, the two sensors are sampling the same geology even though the magnetic data potentially can explore more deeply. The EM-derived susceptibility provides higher spatial resolutions owing to the rapid falloff of the dipolar source field.

2) GEM-2 bistatic ground sensor data. The second example comes from Huang and Won (2000). A GEM-2 handheld sensor was used to investigate environmental problems at a defunct manufactured gas plant in New England. The objectives of the survey included identifying and locating any buried building foundations, abandoned pipelines, isolated objects, and potential contaminant sources and impacted areas. Figure 5 shows maps of (a) the magnetometer data and (b) the apparent susceptibility obtained from 1050 Hz in-phase data.

Three susceptibility highs (A, B, and C), corresponding to known building foundations, are more distinct on the susceptibility map than on the magnetometer map. These highs likely represent metal structures in the foundation. The linear features correspond to the known gas lines connected to the MGP buildings (D) and a storm sewer (E). The gas lines appear on the susceptibility map clearly, but not on the magnetome-
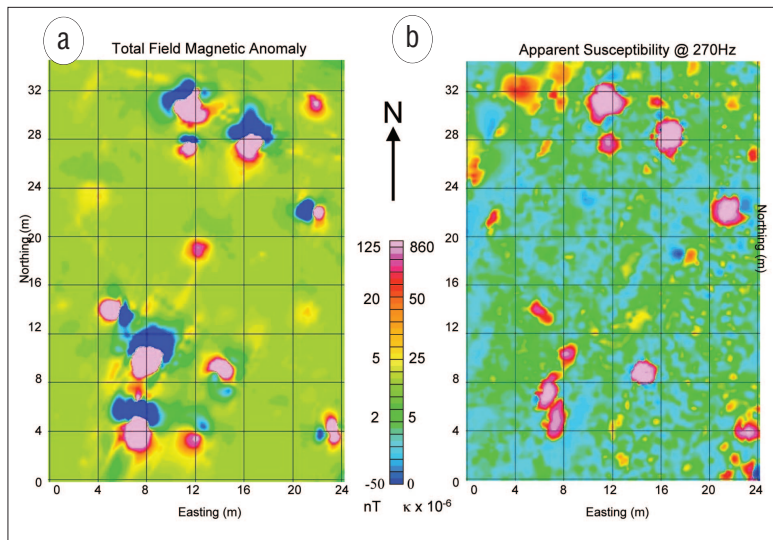
Figure 6. Underwater unexploded ordnance site in the northern San Francisco Bay: (a) total field magnetometer data and (b) apparent susceptibility derived from 270 Hz GEM-3 data.

ter map. Four rectangular features (F) appear on the susceptibility map in the northeastern portion of the site where two features coincide with visible concrete pads on the surface while the other two lack any surface manifestation. Both maps indicate a large circular feature (G) that corresponds to a demolished foundation.

3) Underwater GEM-3 monostatic sensor data. The last example is from an underwater site in the northern San Francisco Bay. The area shown in Figure 6 is a portion of an underwater test site for detecting unexploded ordnance buried in the sediments in a water depth of about 3-4 m. The test involved two separate surveys—one using cesium-vapor magnetometers and the other using the GEM-3 EMI sensor. For each case, a powerboat towed the sensor submerged at a depth of about 2 m below the surface. Each sensor had a GPS antenna mounted directly above for positioning in a differential GPS mode that was estimated to have about decimeter accuracy. To ensure sufficient spatial coverage, the operator monitored a navigation screen that continuously displayed the sensor tracks in real time. In this fashion, one can ensure covering the whole survey area with somewhat evenly distributed tracks on the otherwise featureless water.

The total field magnetic map (Figure 6a) shows many buried ferrous targets indicated by characteristic dipoles that are more pronounced here due to lower magnetic latitudes of this location in comparison with data from two previous examples in Canada and New England. Figure 6b shows the apparent susceptibility map derived from 270 Hz data from the GEM-3. Minor differences between the two maps may be attributed to different sensor tracks, contouring artifacts, and nonferrous targets that are not detected by magnetometers.

One important note: a magnetometer detects both induced and permanent magnetic anomalies without being able to differentiate between the two. On the other hand, an electro-magnetometer can detect only the induced magnetic anomaly. Thus, the difference between the two maps can also be attributed to the two different magnetization effects. This can be a useful feature in certain cases where one wishes to distinguish the degree of permanent versus induced magnetization in a given magnetic geology.

Conclusions. We have shown in this paper, through theory and examples, that a broadband EMI sensor that can also operate at a sufficiently low frequency, or within the resistive limit, can serve as two instruments in one sensor: it can be both a magnetometer and a conductivity meter. Its main disadvantage as a magnetometer is its shallower depth of investigation in comparison with a regular magnetometer that uses the earth's magnetic field as the source. On the other hand, the electro-magnetometer provides higher spatial resolutions for shallow features. Therefore, the dual function is more applicable to near-surface surveys involving environmental and geotechnical investigations than to deep geologic studies.

The dual-mode function would be particularly useful for metal detection (e.g., unexploded ordnance and land mines) by eliminating the need for two separate surveys. It also adds a potential to classify metals as ferrous or nonferrous, in addition to the broadband spectrum that multifrequency EMI sensors can produce as a means of automated target recognition.

Suggested reading. "Magnetic permeability and electrical conductivity mapping with a multifrequency airborne EM system" by Huang and Fraser (*Exploration Geophysics*, 1998). "Airborne resistivity and susceptibility mapping in magnetically polarizable areas" by Huang and Fraser (GEOPHYSICS, 2000). "Mapping of the resistivity, susceptibility, and permittivity of the earth using a helicopter-borne electromagnetic system" by Huang and Fraser (GEOPHYSICS, 2001). "Conductivity and susceptibility mapping using broadband electromagnetic sensors" by Huang and Won (*Journal of Environmental and Engineering Geophysics*, 2001). "Electromagnetic theory for geophysical applications" by Ward and Hohmann (in *Electromagnetic Methods in Applied Geophysics*, SEG, 1988). "GEM-2: A new multifrequency electromagnetic sensor" by Won et al. (*Journal of Environmental and Engineering Geophysics*, 1996). "GEM-3: A monostatic broadband electromagnetic induction sensor" by Won et al. (*Journal of Environmental and Engineering Geophysics*, 1997). TLE

I. J. Won is president of Geophex, a geophysical research and services company based in Raleigh, North Carolina, U.S. He obtained a PhD in geophysics from Columbia University in New York.

Haoping Huang, a research geophysicist at Geophex, studied geophysics at Changchun University in China.

Corresponding author: ijwon@geophex.com; huang@geophex.com